The Astrophysical Journal Letters, 868:L19 (8pp), 2018 December 1 https://doi.org/10.3847/2041-8213/aaef36

Interplanetary Type II Radio Bursts from *Wind*/WAVES and Sustained Gamma-Ray Emission from *Fermi*/LAT: Evidence for Shock Source

Nat Gopalswamy[1], Pertti Mäkelä[1,2], Seiji Yashiro[1,2], Alejandro Lara[1,2], Hong Xie[1,2], Sachiko Akiyama[1,2], and Robert J. MacDowall[1]
[1] NASA Goddard Space Flight Center, Greenbelt, MD 20771, USA
[2] The Catholic University of America, Washington, DC 20624, USA
Received 2018 August 14; revised 2018 October 31; accepted 2018 November 5; published 2018 November 20

Abstract

We present quantitative evidence that interplanetary type II radio bursts and sustained gamma-ray emission (SGRE) events from the Sun are closely related. Out of about 30 SGRE events reported in Share et al. we consider 13 events that had a duration exceeding ~5 hr to exclude any flare-impulsive phase gamma-rays. The SGRE duration also has a linear relation with the ending frequency of the bursts. The synchronism between the ending times of SGRE and the type II emission strongly supports the idea that the same shock accelerates electrons to produce type II bursts and protons (>300 MeV) that propagate from the shock to the solar surface to produce SGRE via pion decay. The acceleration of high-energy particles is confirmed by the associated solar energetic particle (SEP) events detected at Earth and/or at the *Solar Terrestrial Relations Observatory* spacecraft. Furthermore, the presence of >300 MeV protons is corroborated by the fact that the underlying coronal mass ejections (CMEs) had properties identical to those associated with ground-level enhancement events: they had speeds of >2000 km s^{-1} and all were full-halo CMEs. Many SEP events did not have detectable flux at Earth in the >300 MeV energy channels, presumably because of poor magnetic connectivity.

Key words: Sun: coronal mass ejections (CMEs) – Sun: particle emission – Sun: radio radiation – Sun: X-rays, gamma rays

Supporting material: figure set

1. Introduction

Gamma-ray emission extending for hours beyond the flare-impulsive phase (Akimov et al. 1991; Kanbach et al. 1993) is thought to be pion-decay photons from >300 MeV proton interactions. Possible sources of these protons are long-term storage of protons on coronal field lines (Kanbach et al. 1993), and sunward diffusion of protons from coronal/interplanetary shocks (Akimov et al. 1991). The association of gamma-ray line emission (GRL) with type II radio bursts and fast coronal mass ejections (CMEs) has been contemplated for quite some time (Bai & Dennis 1985; Ramaty et al. 1987; Cliver et al. 1989). GRL emission observed on the visible disk from the 1989 September 29 backside eruption warranted a shock source (Cliver et al. 1993). The Large Area Telescope (LAT; Ajello et al. 2014) on board the *Fermi* satellite has shown that the extended-duration gamma-ray events are very common (Ackermann et al. 2014, 2017; Share et al. 2017; Klein et al. 2018; Omodei et al. 2018). Such sustained gamma-ray emission (SGRE) lasting for several hours after the flare-impulsive phase certainly require a CME-driven shock, and this became clear when LAT observed gamma-ray emission from backside eruptions (Pesce-Rollins et al. 2015; Ackermann et al. 2017; Plotnikov et al. 2017; Jin et al. 2018).

Type II radio bursts are caused by nonthermal electrons accelerated at coronal/interplanetary (IP) shocks (Gopalswamy et al. 2001a; Vršnak et al. 2001; Reiner et al. 2007). Bursts with emission components in the metric (m) to kilometric (km) wavelengths are due to CMEs with the highest energy (Gopalswamy et al. 2005), and the CME properties are similar to those associated with large solar energetic particle (SEP) events (Gopalswamy 2006). The SEP association rate of IP type II bursts originating from the western hemisphere of the Sun is 100% when the CME speed is ⩾1800 km s^{-1} (Gopalswamy et al. 2008). Unlike SEP events, type II bursts are not affected by magnetic connectivity, so they can be readily observed from anywhere on the Sun and even from eruptions that are tens of degrees behind the limb. The starting frequency of type II bursts indicates the shock-formation distance from the Sun that can range from ~1.2 solar radii (Rs) to >100 Rs (Gopalswamy et al. 2010a, 2013b, 2015, 2017; Mäkelä et al. 2015). Occasionally, the shock-formation heights can even be closer to the Sun (e.g., Pohjolainen et al. 2008). The ending frequency of type II bursts indicates the distance traveled by the shock before becoming weak and radio-quiet, and hence has implications for the duration of SGREs.

In this Letter, we consider SGREs exceeding ~5 hr to be definitive that there are no impulsive-flare emission. We compare the SGRE duration with the duration and ending frequencies of the associated IP type II bursts to show a quantitative relationship that points to the common shock source. We also investigate the properties of the underlying CMEs that further confirm the acceleration of high-energy particles required for SGREs.

2. Data

Share et al. (2017) reported 30 SGRE events, of which 14 had durations exceeding ~5 hr. We dropped the 2014 September 1 backside event because the duration is uncertain. We identified the associated CME, flare, and type II burst for

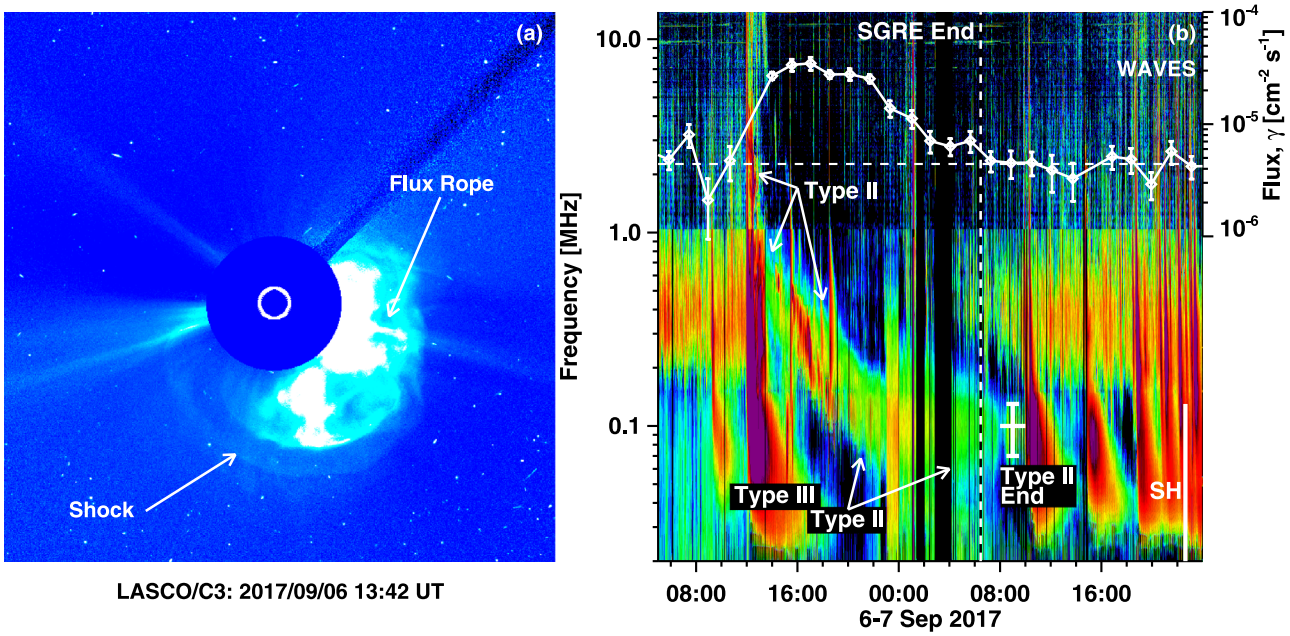

Figure 1. (a) *SOHO*/LASCO CME with shock and flux rope. (b) *Wind*/WAVES type II burst starting around 14 MHz (~12:05 UT, September 6) and continuing down to ~100 kHz (09:00 UT, September 7). The end time is marked by the short vertical line with its length indicating the bandwidth (70–130 kHz). The horizontal tick marks the end time uncertainty. The vertical dashed line marks the SGRE end (06:28 UT, September 7); the horizontal dashed line marks the gamma-ray background. The shock arrival time at 1 au is marked "SH." The dynamic spectra with SGRE light curve for all other events are shown in Figure 5 and in the online supplementary material.

the remaining 13 events. The CMEs were observed by the Large Angle and Spectrometric Coronagraph (LASCO; Brueckner et al. 1995) on board the *Solar and Heliospheric Observatory* (*SOHO*) and the Sun Earth Connection Coronal and Heliospheric Investigation (Howard et al. 2008) on board the *Solar Terrestrial Relations Observatory* (*STEREO*). Type II bursts were recorded by the Radio and Plasma Wave Experiment (WAVES; Bougeret et al. 1995) on board the *Wind* spacecraft. We refine the type II end times from the list https://cdaw.gsfc.nasa.gov/CME_list/radio/waves_type2.html. The sky-plane (V_{sky}) and (V_{cone}) deprojected speeds CMEs are from the CDAW catalog: (https://cdaw.gsfc.nasa.gov/CME_list). The peak value of the three-dimensional (3D) speeds (V_{pk}) are obtained using the graduated cylindrical shell fit (Thernisien 2011) as reported in previous publications (Gopalswamy et al. 2014, 2016, 2018a, 2018b).

Figure 1 shows the 2017 September 6 fast (~1570 km s^{-1}) halo CME from S08W33 associated with an X9.3 flare, a shock and a type II radio burst. The type II burst ended around 08:00 UT with a possible extension until ~10 UT, giving a mean duration (t_{t2}) of 20.92 ± 1.0 hr. The SGRE start time is taken as the soft X-ray peak time (12:02 UT) to avoid the impulsive phase; the end time is defined as the mid-time (06:28 UT) between the last data point above the gamma-ray background (05:39 UT) and the next data point (07:16 UT). Thus, the SGRE duration (t_{SGRE}) is (18.43 ± 0.8) hr. We used the gamma-ray background level available online (https://hesperia.gsfc.nasa.gov/fermi_solar/). The uncertainties are half the orbit period in most cases, but longer if the Sun was not visible to *Fermi* during an orbit. Figure 1 demonstrates that SGRE ends when the type II burst ends.

We extend the SGRE connection to type II burst, CME, SEP event, and flare demonstrated in Figure 1 to all 13 SGRE events. Table 1 lists details on SGRE (columns 1–3), CME (columns 4–7), soft X-ray flare (columns 8–11), SEP event (columns 12–13), and type II burst (columns 14–21). A suffix "H" to V_{sky} indicates that the CME is a halo CME. The >10 MeV proton intensity (column 10) in large SEP events is from https://cdaw.gsfc.nasa.gov/CME_list/sepe/; in minor events (intensity <10 pfu), we determined the peak flux from *GOES* data. The numbers in parentheses denote the >10 MeV flux from *STEREO*—Behind (STB). Column 11 notes whether or not a detectable signal in a >300 MeV *GOES* energy channel exists (N = No, Y = Yes). The onset times of metric type II bursts (column 12) are either from the online Solar Geophysical Data or from our own examination of the dynamic spectra from radio observatories. The onset times of decameter-hectometric (DH) type II bursts (column 13) are from the CDAW Data Center (https://cdaw.gsfc.nasa.gov/CME_list/radio/waves_type2.html). The end times (column 14) are obtained by examining the *Wind*/WAVES type II bursts as the time when the bursts either ended or weakened significantly. Column 15 (end2) denotes the upper limit of the ending time. The upper (f_2) and lower (f_1) edges of the type II band at f_1 and the ending frequency [$f_{t2} = (f_1 + f_2)/2$)] are listed in columns 16, 17, and 18, respectively. The SGRE durations (column 3), DH type II burst durations (column 18), and f_{t2} (column 21) are the main parameters used in this study. In two events, the ending times/frequencies are not reliable because of an intense low-frequency background in one case (2012 March 9) and a faint, fragmented emission in the other (2013 May 14). These events occurred in clusters with preceding CMEs and elevated SEP background. We consider only type II bursts in the IP medium (DH wavelengths and beyond) because metric type II bursts indicate shock formation, but it takes ~10 minutes to accelerate high-energy particles after the shock has formed (Reames 2009; Gopalswamy et al. 2012).

Table 1
Properties of SGREs and the Associated CMEs, Type II Bursts, and SEP Events

SGRE (Columns 1–3)			CME (Columns 4–7)				Flare (Columns 8–11)				Large SEP (Columns 12–13)		Type II Radio Burst (Columns 14–21)						
Start UT[a]	End UT	Dur. hr	UT	V_{sky} km s^{-1}	V_{cone} km s^{-1}	V_{pk} km s^{-1}	Location	Class	Start UT	Peak UT[e]	>10 MeV[f] pfu	>300 MeV[g]	Metric	DH Start UT	DH End UT	DH End2 UT	Dur. hr	f_1	f_2	f_{t2}
2011 Mar 7 20:00	15:44[b]	19.54 ± 3.03	20:00	2125H	2223	2660	N31W53	M3.2	19:43	20:12	50	N	19:54	03/07 20:00	03/08 08:30	03/08 09:50	13.17 ± 0.67	180	250	215
2012 Jan 23 04:20	19:25	15.43 ± 0.83	04:00	2175H	2511	2150	N28W21[c]	M8.7	03:38	03:59	6310	Y?	03:38	01/23 04:00	01/23 19:25	01/24 14:33[h]	24.99 ± 9.57	50	90	70
2012 Mar 5 04:30	08:24	4.25 ± 0.80	04:00	1531H	1627	1628	N17E52[c]	X1.1	03:17	04:09	4 (100 HiB)	N	…	03/05 04:00	03/05 09:55	03/05 12:04	7.0 ± 1.10	350	410	380
2012 Mar 7 02:00	21:40	21.27 ± 1.64	00:24	2684H	3146	2987	N17E27[c]	X5.4[d]	00:02	00:24	6350	Y	00:17	03/07 00:30	03/07 21:40	03/08 10:53[h]	27.93 ± 6.76	35	90	63
2012 Mar 9 04:30	14:19	10.44 ± 2.15	04:26	0950H	1229	1737	N15W03	M6.3	03:22	03:53	600 HiB	Y?	03:43	03/09 04:00	03/09 06:05	03/09 09:30	3.8[i] ± 1.72	…	…	…
2012 Mar 10 20:00	05:21[b]	11.61 ± 1.59	18:00	1296H	1638	2157	N17W24[c]	M8.4	17:15	17:44	120 HiB	Y?	…	03/10 17:55	03/11 00:55	03/11 01:45	7.42 ± 0.42	160	220	190
2013 May 13 17:00	00:46[a]	8.68 ± 0.95	16:07	1850H	1852	2889	N11E85[c]	X2.8	15:48	16:05	1 (400 HiB)	N	15:57	05/13 16:15	05/14 00:40	05/14 01:00	8.58 ± 0.17	210	250	230
2013 May 14 01:20	07:10	5.98 ± 0.82	01:25	2625H	2645	2963	N08E77	X3.2	00:00	01:11	1 (608 HiB)	N	01:07	05/14 01:16	05/14 06:40	05/14 08:20	6.23[j] ± 0.83	240	280	260
2013 May 15 02:00	05:24	3.60 ± 0.82	01:48	1366H	1408	2294	N12E64[c]	X1.2	01:25	01:48	42	N	01:37	05/15 01:49	05/15 07:57	05/15 08:30	6.42 ± 0.28	230	340	285
2014 Feb 25 00:50	09:17	8.46 ± 1.59	01:25	2147H	2153	2777	S12E82	X4.9	00:39	00:49	24 (400)	Y	00:56	02/25 00:56	02/25 10:30	02/25 12:00	10.32 ± 0.75	210	300	255
2015 Jun 21 02:20	16:40	14.06 ± 1.61	02:36	1366H	1740	2119	N12E16	M2.6	02:06	02:36	1066	N	02:24	06/21 02:33	06/21 22:00	06/22 01:00	20.95 ± 1.50	160	220	190[k]
2017 Sep 6 12:35	06:28[b]	18.43 ± 0.80	12:24	1571H	1884	2000	S08W33[c]	X9.3	11:53	12:02	844 HiB	Y?	12:02	09/06 12:05	09/07 08:00	09/07 10:00	20.92 ± 1.00	70	130	100
2017 Sep 10 15:56	07:17[b]	15.18 ± 0.81	16:00	3163H	3165	4191	S09W92[c]	X8.3	15:35	16:06	1490	Y	15:53	09/10 16:02	09/11 06:50	09/11 08:40	15.72 ± 0.92	150	190	170[l]

Notes.
[a] Times given by Share et al. (2017), not used in computing the SGRE duration; the 2013 May 15 event had a duration >5 hr in Share et al. (2017), but the duration turned out to be 3.6 hr based on our criterion.
[b] Time corresponds to the next day.
[c] Interacting event.
[d] The eruption was followed by an X1.3 flare and a fast CME (1825 km s^{-1}), but slower than the preceding one.
[e] Peak time of the soft X-ray flare taken as the start time of SGRE for computing the SGRE duration.
[f] The numbers in parentheses are >10 MeV flux from STB data by extrapolating the spectrum to 150 MeV; HiB = high background, so the estimated intensity is approximate.
[g] N = No; Y = Yes; the question mark indicates that the signal is extremely weak.
[h] Shock arrival time at Earth.
[i] Type II duration is uncertain because of intense background below 500 kHz.
[j] Type II burst is fragmented and weak.
[k] Fragmented emission observed until the *Wind* shock arrival at 22/18:01 UT.
[l] WAVES data gap on 9/10, but *STEREO* WAVES data show type II emission in the gap.

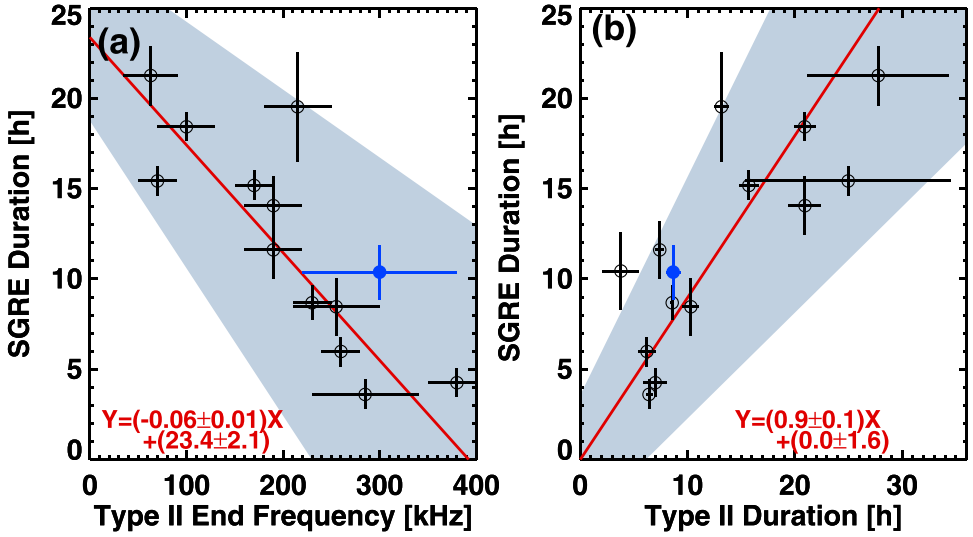

Figure 2. Scatter plots of SGRE duration with type II ending frequency (a) and type II duration (b). The best-fit lines (red) are obtained using the Orthogonal Distance Regression method, which considers errors in both *X* and *Y* variables. The shaded area represents 95% confidence interval of the fit. The 1991 June 11 Energetic Gamma Ray Experiment Telescope (EGRET) event (not included in the fit) is denoted by the blue symbols, which are consistent with the linear relationship.

3. Analysis and Results

3.1. Properties of the Associated CMEs

Table 1 shows that the CMEs associated with the 13 SGRE events are all very fast with an average sky-plane speed of $1912 \pm 646\,\mathrm{km\,s^{-1}}$, slightly above the average speed ($\sim$1500 $\mathrm{km\,s^{-1}}$) of SEP-associated CMEs (see e.g., Gopalswamy et al. 2004). The deprojected speeds average to $2094 \pm 621\,\mathrm{km\,s^{-1}}$, while the peak speeds average to $2504 \pm 682\,\mathrm{km\,s^{-1}}$. In addition, all 13 CMEs (100%) were halo CMEs (those that appear to surround the occulting disk of the coronagraph in sky-plane projection; Howard et al. 1982). For a given coronagraph, halo CMEs are indicative of an energetic population (Gopalswamy et al. 2010b). The speeds and halo fractions of SGRE CMEs are properties shared by ground-level enhancement (GLE) events, in which particles are accelerated to GeV energies. The average speed of GLE CMEs is $>2000\,\mathrm{km\,s^{-1}}$ and all but two of the 18 GLEs (88%) in solar cycles 23 and 24 are halos (Gopalswamy et al. 2016). Another property shared by SGRE and GLE events is that the associated DH type II bursts extend to kilometric wavelengths (see Table 1). The extreme CME properties in SGRE events are thus indicative of copious levels of >300 MeV protons needed for SGRE. Not all SGRE events have GLEs because the latter need to have magnetic connectivity to Earth to be detected.

3.2. Association with Type II Radio Bursts

The type II burst durations (t_{t2}) range from 3.80 to 27.93 hr (average: 13.34 ± 7.99 hr), very similar to the SGRE durations (average: 12.07 ± 5.80 hr). The ending frequencies (f_{t2}) range from 63 to 380 kHz (average: 200.7 ± 92.5 kHz). For comparison, the typical local plasma frequency at the *Wind* spacecraft (Sun–Earth L1 point) is $\sim$30 kHz. The average ending frequency corresponds to a local plasma density of $\sim$500 $\mathrm{cm^{-3}}$. Such a density prevails at a heliocentric distance of tens of Rs. For example, ending frequency ($\sim$190 kHz) in the 2015 June 21 event corresponds to a heliocentric distance of $\sim$90 Rs (Gopalswamy et al. 2018a).

The scatter plots of SGRE duration with f_{t2} and t_{t2} in Figure 2 show linear relationships (f_{t2} and t_{t2} are related, so the correlations are complementary). The $f_{t2} - t_{SGRE}$ best-fit line has a negative slope because the plasma density and hence the emission frequency is lower at larger heliocentric distances. The regression lines were obtained using the Orthogonal Distance Regression method (see, e.g., Oliveira & Aguiar 2013) suitable when both *X* and *Y* variables have errors. Figure 2 shows that all of the data points are within the 95% confidence interval of the best-fit line, except for one data point (2012 March 9); as noted before, this event had intense low-frequency background so the type II duration and ending frequencies were not determined accurately. Thus, in longer-duration SGRE events, the shock remains stronger over a larger distance from the Sun. Figure 2 supports the idea that DH type II duration (and hence the duration over which the shock efficiently accelerates particles) is a good indicator of SGRE. Physically speaking, the same shock accelerates protons responsible for SGRE and electrons responsible for the type II bursts. A reverse study is underway to check the gamma-ray association of all DH type II bursts observed after the launch of *Fermi*.

3.3. SEP Association

All SGRE events were associated with SEP events, but three of the eastern events were minor (>10 MeV intensity at Earth <10 pfu, see Table 1) presumably because of poor connectivity. These and other eastern-hemisphere events were intense >10 MeV SEP events at STB. Share et al. (2017) were able to compare the durations of >100 MeV protons with the SGRE durations in only 10 events. Of these, only two events had SGRE durations >3.5 hr, so we cannot do any statistics. However, we can show that it is highly likely that the required high-energy protons were present in our events. Intense eastern-hemispheric SEP events generally have a soft spectrum because only the shock flanks are connected to Earth (e.g., Gopalswamy et al. 2016). This is the reason that GLE CMEs generally originate from the western hemisphere of the Sun, where the longitudinal connectivity is better. Western CMEs with very high initial speeds produce hard SEP events (Gopalswamy et al. 2016), so it is highly likely that >300 MeV protons were present in these events. The 2014 February 25 CME had speeds exceeding $2000\,\mathrm{km\,s^{-1}}$ (see Table 1). The

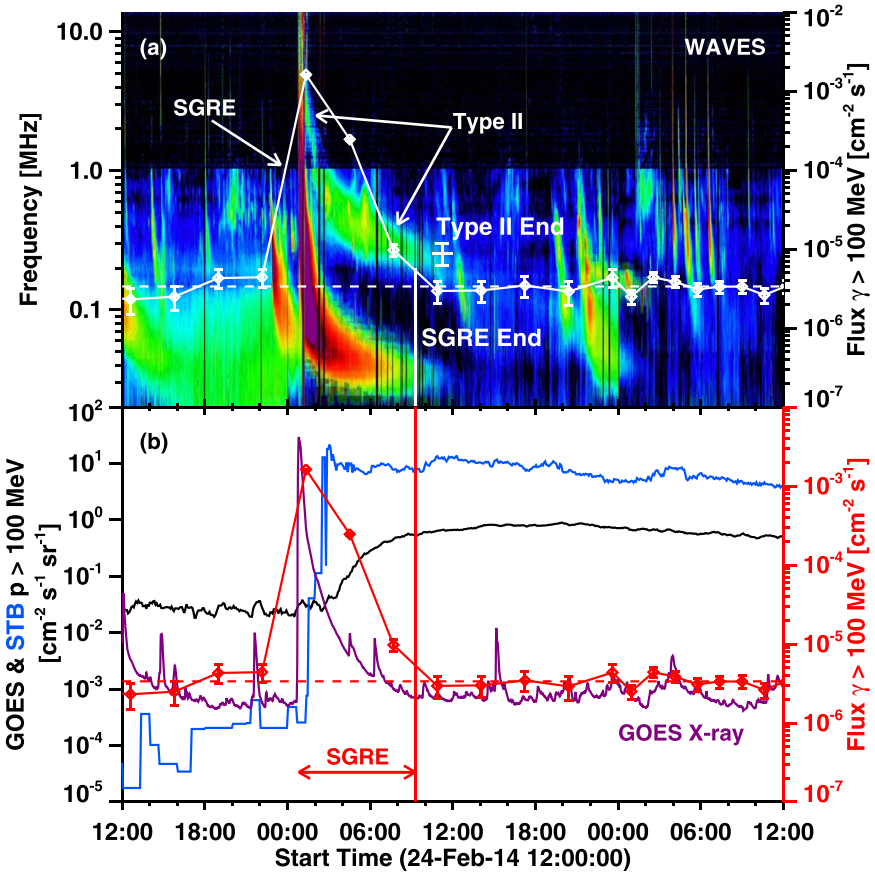

Figure 3. (a) Type II burst and SGRE during the 2014 February 25 CME showing synchronous ending. (b) >100 MeV proton intensity from *GOES* (black) and STB (blue) compared with the 1–8 Å *GOES* soft X-ray (arbitrary units) and SGRE (red) light curves. The SGRE duration is marked by the double arrow. STB was located at E160 and hence well connected to the solar source at S12E82.

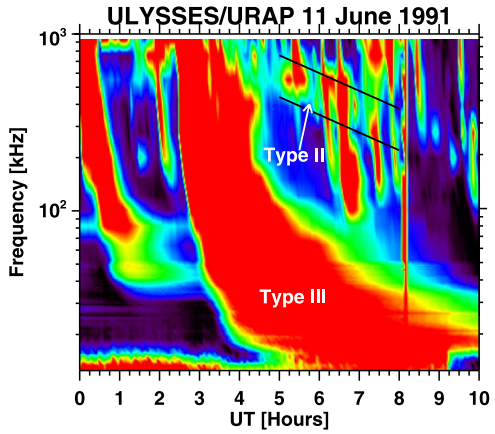

Figure 4. *Ulysses*/URAP type II burst during the 1991 June 11 SGRE. The two black lines roughly mark the edges of the type II burst. The intense type III burst is typical of energetic CMEs. There are also short-duration type III bursts superposed on the type II emission. The long vertical feature after 8:00 UT marks a data gap. Data from ftp://ftp.cosmos.esa.int/ULYSSES/URAP/data/.

initial speed from STB images obtained by the Extreme Ultraviolet Imager (EUVI) and the inner coronagraph COR1 was ~2300 km s^{-1}. We do not expect a GLE, however, because of the poor connectivity (source at S12E82). The >10 MeV intensity was only ~24 pfu at Earth, but ~400 pfu at the well-connected STB. To compute the >100 MeV proton intensity, we extrapolated the SEP spectra obtained from STB particle data, assuming that no particles were present beyond 1 GeV. The resulting >100 MeV intensity is compared with that from *GOES* in Figure 3: the *GOES* intensity increased gradually to reach a peak level of ~1 pfu, whereas the STB intensity rose promptly and reached >10 pfu. The >100 MeV intensity remained high when the type II emission and SGRE were above the background, as illustrated in Figure 3.

Winter et al. (2018) highlighted the 2011 March 7 SGRE event as a counter example to the shock-source idea because there were no >300 MeV protons above the background. We think the lack of >300 MeV signal at Earth is probably due to poor latitudinal connectivity. For an SEP event to be a GLE, the ecliptic distance of the shock nose should be ~13° (Gopalswamy et al. 2013a, 2014, 2018b; Gopalswamy & Mäkelä 2014). This happens when the highest-energy particles are accelerated at the shock nose. In the 2011 March 7 event, the CME nose was at position angle (PA) 313°, which is ~43° away from the equator, consistent with a northern (N31W53) source and an unfavorable solar B0 angle (−7.°25). The nose area, where >300 MeV particles are accelerated, is expected to be larger than that for GeV particles, but should not reach as far as 43°. Thus, despite the good longitudinal connectivity (W53), the poor latitudinal connectivity seems to be a plausible explanation for not observing >300 MeV particles at Earth, but they can flow from the shock nose toward the solar surface to produce the observed SGRE. In the 2012 January 23 event, >300 MeV particles were barely detected at Earth. The CME nose was at PA = 326° consistent with the source location,

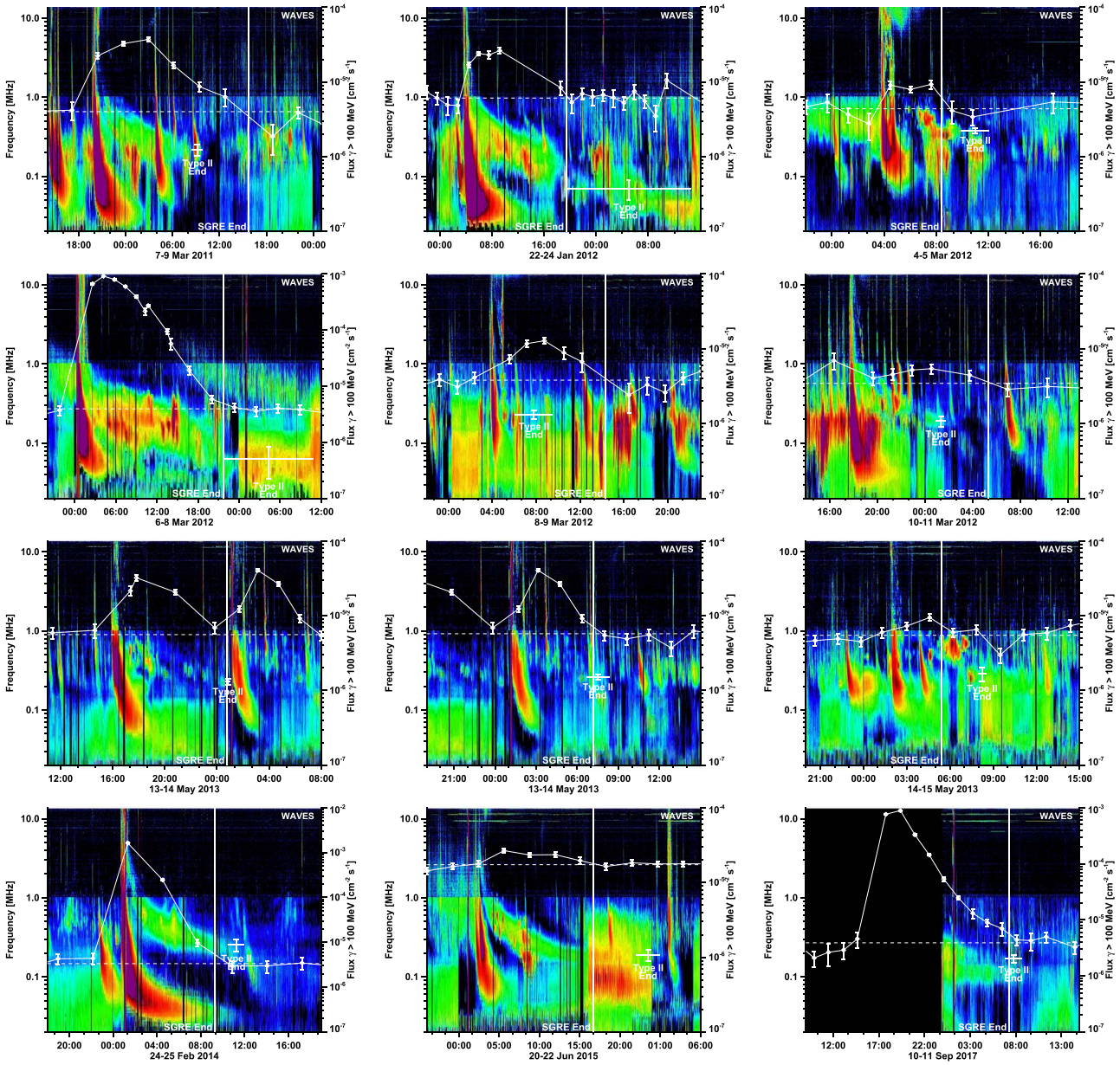

Figure 5. *Wind*/WAVES dynamic spectra of all SGRE events investigated in the work. Each panel shows (i) the type II burst with its end time, end frequency, and bandwidth marked, (ii) SGRE light curve, and (iii) a vertical line indicating the end time of the gamma-ray event. Table 1 was created using these figures. The 2017 September 6 event is excluded, as it is already in Figure 1(b).

(The complete figure set (12 images) is available.)

N28W21. The 110–900 MeV *GOES* channel did have a weak signal indicating a wider nose. The CME interacted with a preceding CME that is similar to seven other events (see Table 1). It is possible that the preceding CME causes a localized constriction of the magnetic field lines leading to mirroring of particles toward the Sun—a scenario often invoked in GLE events (Bieber et al. 2002). Most of the events occurred when there was elevated background from preceding eruptions suggesting the availability of seed particles. These aspects need further investigation.

3.4. *The Pre*-Fermi *SGRE*

The 1991 June 11 SGRE was detected by the Energetic Gamma Ray Experiment Telescope (EGRET) on board the Compton Gamma Ray Observatory (Kanbach et al. 1993; Ryan 2000). The eruption was associated with intense H-alpha and *GOES* (X12) flares and a metric type II burst at 02:05 UT. From the X12 flare peak (02:09 UT) to the last interval of significant gamma-ray flux (11:02–14:02 UT, see Kanbach et al. 1993, their Table 1) we estimate the duration as 10.38 ± 1.5 hr. The duration is slightly larger than that (8.33 hr) in Chupp & Ryan (2009) because of the criterion that we used. Pioneer Venus Orbiter (PVO) detected a 780-km s^{-1} shock about 27 hr after the eruption (Mihalov & Strangeway 1995). Because PVO was at E45, the shock should have been faster at Earth, $\sim$1100 km s^{-1}. A shock with such high speed at Earth might have had a CME initial speed of $\sim$1700 km s^{-1}, assuming typical interplanetary acceleration (Gopalswamy et al. 2001b).

A DH type II burst was detected by the Unified Radio and Plasma waves experiment (URAP; MacDowall et al. 1996) on board the *Ulysses* mission (Figure 4). The burst drifts from ~900 kHz at ~5 UT to ~300 KHz at 8:00 UT, possibly extending to ~9:20 UT. The burst is faint, fragmented, and barely discernible because *Ulysses* was ~3.30 au from the Sun. The complex type III burst that typically occurs at the IP type II onset, started at 02:20 UT (Earth onset at 02:01 UT because the signal has to travel an additional 2.3 au to arrive at *Ulysses*). Thus we obtain the type II duration was $\sim 8.67 \pm 0.67$ hr, which is similar to the SGRE duration. The *Ulysses* type II burst and the EGRET SGRE are consistent with the linear relationships in Figure 2 (also evident from the *Wind*/WAVES dynamic spectra in Figure 5 with overlaid SGRE light curves). The 1991 June 11 GLE (Smart et al. 1994) confirms the presence of the required >300 MeV particles. Solar Geophysical Data reported significant fluxes in the highest *GOES* energy channel, 640–850 MeV (Coffey 1991). Thus, the EGRET event is consistent with the *Fermi*/LAT SGRE events in their relationship with IP type II burst durations.

4. Discussion and Summary

Although the association between SGREs and IP type II bursts have been noted before (Share et al. 2017; Klein et al. 2018), we have established a quantitative relation between them: the SGRE ends roughly when the type II ends. The linear relation between SGRE and IP type II durations at 95% confidence level supports the idea that the protons responsible for SGRE and electrons that produce the type II bursts are accelerated by the same shock. The accelerated protons propagate toward the Sun and precipitate to the chromosphere, where the pions are produced. A preliminary look at the shorter-duration SGRE events confirm the results of this Letter. A detailed analysis of those events will be reported elsewhere. The present observations should provide strong constraints on the propagation of high-energy protons from the outer corona and interplanetary medium toward the Sun. One also needs to investigate issues such as magnetic mirroring and the presence of enhanced seed particles in interacting events. In intense events (2012 January 23 and March 7), there was type II emission after a clear break at the SGRE end. These may indicate the difference in accelerating ~10 keV electrons (for type II) and >300 MeV protons (for SGRE). Investigation of these events will further clarify the sites of particle acceleration on the shock surface.

The main results of this Letter can be summarized as follows.

1. All SGRE events were associated with interplanetary type II bursts in the decameter to kilometer wavelength domains, indicating strong shocks propagating far into the heliosphere.
2. The CMEs associated with SGRE are among the most energetic, a property shared by GLE events: the average CME speed exceeded 2000 km s^{-1}, all (100%) were halos, and all were associated with type II bursts extending to km wavelengths. The similarity to GLE events is important because, if GeV particles are accelerated, the presence of >300 MeV particles is assured.
3. The durations of IP type II radio bursts and SGRE have a linear relationship, suggesting that the same shock is responsible for accelerating both electrons and protons, the underlying energetic particles in the two electromagnetic emissions.
4. The ending frequency of IP type II bursts has an inverse linear relation with SGRE duration confirming that in longer-duration gamma-ray events the IP shocks remaining strong over larger distances from the Sun (where the local plasma frequency is lower).
5. SEP events were associated with each of the SGRE events, but >300 MeV particles were not detected in most of the events presumably because of poor magnetic connectivity to Earth in longitude and latitude.
6. All SGRE events originating from the eastern hemisphere of the Sun were associated with large SEP events observed by the *STEREO* spacecraft.
7. The only >5 hr SGRE event from EGRET (1991 June 11) was also associated with a long-lasting *Ulysses*/URAP type II burst consistent with *Fermi*/LAT SGRE events.

This Letter benefited from NASA's open data policy in using *Fermi Wind*, *SOHO*, and *SDO* data and NOAA's *GOES* X-ray and particle data. *SOHO* is a joint project of ESA and NASA. We thank A. K. Tolbert and J. M. Ryan for helpful discussions, and E. W. Cliver, G. H. Share, and B. R. Dennis for reading the manuscript and providing helpful comments. Work supported by NASA's LWS TR&T and heliophysics GI programs.

ORCID iDs

Nat Gopalswamy https://orcid.org/0000-0001-5894-9954
Pertti Mäkelä https://orcid.org/0000-0002-8182-4559
Seiji Yashiro https://orcid.org/0000-0002-6965-3785
Sachiko Akiyama https://orcid.org/0000-0002-7281-1166
Robert J. MacDowall https://orcid.org/0000-0003-3112-4201

References

Ackermann, M., Ajello, M., Albert, A., et al. 2014, ApJ, 787, 15
Ackermann, M., Allafort, A., Baldini, L., et al. 2017, ApJ, 835, 219
Ajello, M., Albert, A., Allafort, A., et al. 2014, ApJ, 789, 20
Akimov, V. V., Afanassyev, V. G., Belaousev, A. S., et al. 1991, Proc. ICRC (Dublin), 3, 73
Bai, T., & Dennis, B. R. 1985, ApJ, 292, 699
Bieber, J. W., Dröge, W., Evenson, P. A., et al. 2002, ApJ, 567, 622
Bougeret, J.-L., Kaiser, M. L., Kellogg, P. J., et al. 1995, SSRv, 71, 231
Brueckner, G. E., Howard, R. A., Koomen, M. J., et al. 1995, SoPh, 162, 357
Chupp, E. L., & Ryan, J. M. 2009, RAA, 9, 11
Cliver, E. W., Forrest, D. J., Cane, H. V., et al. 1989, ApJ, 343, 953
Cliver, E. W., Kahler, S. W., & Vestrand, W. T. 1993, Proc. ICRC (Alberta), 3, 91
Coffey, H. E. 1991, Solar-Geophysical Data Number 563, Part 1 (Prompt Rep.)
Gopalswamy, N. 2006, in Solar Eruptions and Energetic Particles, Geophysical Monograph, Vol. 165, ed. N. Gopalswamy et al. (Washington, DC: AGU), 207
Gopalswamy, N., Aguilar-Rodriguez, E., Yashiro, S., et al. 2005, JGRA, 110, A12S07
Gopalswamy, N., Lara, A., Yashiro, A., Kaiser, M. L., & Howard, R. A. 2001a, JGRA, 106, 29207
Gopalswamy, N., & Mäkelä, P. 2014, in ASP Conf. Ser. 484, Latitudinal Connectivity of Ground Level Enhancement Events, In: Outstanding Problems in Heliophysics: from Coronal Heating to the Edge of the Heliosphere, ed. Q. Hu & G. P. Zhang (San Francisco, CA: ASP), 63
Gopalswamy, N., Mäkelä, P., Akiyama, S., et al. 2015, ApJ, 806, 8
Gopalswamy, N., Makela, P., Akiyama, S., et al. 2018a, JASTP, 179, 225
Gopalswamy, N., Mäkelä, P., Yashiro, S., et al. 2017, JPhCS, 900, 012009
Gopalswamy, N., Xie, H., Akiyama, S., et al. 2013a, ApJL, 765, L30
Gopalswamy, N., Xie, H., Akiyama, S., Mäkelä, P., & Yashiro, S. 2014, EP&S, 66, 104
Gopalswamy, N., Xie, H., Mäkelä, P., et al. 2010a, ApJ, 710, 1111

Gopalswamy, N., Xie, H., Mäkelä, P., et al. 2013b, AsSpR, 51, 1981
Gopalswamy, N., Xie, H., Yashiro, S., et al. 2012, SSRv, 171, 23
Gopalswamy, N., Yashiro, S., Akiyama, S., et al. 2008, AnGeo, 26, 3033
Gopalswamy, N., Yashiro, S., Kaiser, M. L., Howard, R. A., & Bougeret, J.-L. 2001b, JGRA, 106, 29219
Gopalswamy, N., Yashiro, S., Krucker, S., Stenborg, G., & Howard, R. A. 2004, JGR, 109, A12105
Gopalswamy, N., Yashiro, S., Makela, P., et al. 2018b, ApJL, 863, L39
Gopalswamy, N., Yashiro, S., Michalek, G., et al. 2010b, SunGe, 5, 7
Gopalswamy, N., Yashiro, S., Thakur, N., et al. 2016, ApJ, 833, 216
Howard, R. A., Michels, D. J., Sheeley, N. R., & Koomen, M. J. 1982, ApJL, 263, L101
Howard, R. A., Moses, J. D., Vourlidas, A., et al. 2008, SSRv, 136, 67
Jin, M., Petrosian, V., Liu, W., et al. 2018, ApJ, 867, 122
Kanbach, G., Bertsch, D. L., Fichtel, C. E., et al. 1993, A&AS, 97, 349
Klein, K.-L., Tziotziou, K., Zucca, P., et al. 2018, Astrophysics and Space Science Library, 444, 133
MacDowall, R. J., Hess, R. A., Lin, N., et al. 1996, A&A, 316, 396
Mäkelä, P., Gopalswamy, N., Akiyama, S., Xie, H., & Yashiro, S. 2015, ApJ, 806, 13
Mihalov, J. D., & Strangeway, R. J. 1995, SoPh, 160, 363
Oliveira, E. C., & Aguiar, P. F. 2013, Quím. Nova, 36, 885
Omodei, N., Pesce-Rollins, M., Longo, F., Allafort, A., & Krucker, S. 2018, ApJL, 865, L7
Pesce-Rollins, M., Omodei, N., Petrosian, V., et al. 2015, ApJL, 805, L15
Plotnikov, I., Rouillard, A. P., & Share, G. H. 2017, A&A, 608, A43
Pohjolainen, S., Pomoell, J., & Vainio, R. 2008, A&A, 490, 357
Ramaty, R., Murphy, R. J., & Dermer, C. D. 1987, ApJL, 316, L41
Reames, D. V. 2009, ApJ, 693, 812
Reiner, M. J., Kaiser, M. L., & Bougeret, J.-L. 2007, ApJ, 663, 1369
Ryan, J. M. 2000, SSRv, 93, 581
Share, G. H., Murphy, R. J., Tolbert, A. K., et al. 2017, ApJS, in press (arXiv:1711.01511)
Smart, D. F., Shea, M. A., & Gentile, L. C. 1994, in AIP Conf. Proc. 294, High-energy Solar Phenomena: A New Era of Spacecraft Measurements, ed. J. M. Ryan & W. T. Vestramd (Melville, NY: AIP), 222
Thernisien, A. 2011, ApJS, 194, 33
Vršnak, B., Aurass, H., Magdalenić, J., & Gopalswamy, N. 2001, A&A, 377, 321
Winter, L. M., Bernstein, V., Omodei, N., & Pesce-Rollins, M. 2018, ApJ, 864, 39